JOURNAL OF COMPUTATIONAL PHYSICS **129,** 160–169 (1996)
ARTICLE NO. 0240

A Numerical Method for Solution of the Generalized Liouville Equation

J. Candy

JET Joint Undertaking, Abingdon, Oxfordshire OX14 3EA, United Kingdom

Received September 13, 1995; revised April 25, 1996

A numerical method for the time evolution of systems described by Liouville-type equations is derived. The algorithm uses a lattice of numerical markers, which follow exactly Hamiltonian trajectories, to represent the operator d/dt in moving (i.e., Lagrangian) coordinates. However, nonconservative effects such as particle drag, creation, and annihilation are allowed in the evolution of the physical distribution function, which is itself represented according to a δf decomposition. Further, the method is suited to the study of a general class of systems involving the resonant interaction of energetic particles with plasma waves. Detailed results are presented for both the classic bump-on-tail problem and the beam-driven TAE instability. In both cases, the algorithm yields exceptionally smooth, low-noise evolution of wave energy, especially in the linear regime. Phenomena associated with the nonlinear regime are also described.

1. INTRODUCTION AND BACKGROUND

1.1. *The Liouville Equation*

Consider a distribution function f which describes an ensemble of particles (or more generally, an ensemble of system points) following a Hamiltonian flow in the phase space Γ:

$$f = f(\Gamma, t) \quad \text{with } \Gamma \equiv (q_1, ..., q_N; p_1, ..., p_N). \tag{1}$$

The number of system points in the phase volume element $d\Gamma$ at time t is $f(\Gamma, t)\, d\Gamma$. If these points are neither created nor destroyed, the distribution function f must satisfy the *Liouville equation*

$$\frac{df}{dt} = 0. \tag{2}$$

Thus, the "fluid" of system points in this case moves incompressibly. In fact, the motion is more than simply incompressible; because the phase space Γ is Hamiltonian, it will always possess a hierarchy of N integral invariants, the first and Nth of which are

$$\int_{\text{proj}\{\Delta\Gamma[t],1\}} dq_1\, dp_1 + \cdots + \int_{\text{proj}\{\Delta\Gamma[t],N\}} dq_N\, dp_N = \text{const}, \tag{3a}$$

$$\int_{\Delta\Gamma[t]} dq_1 \cdots dq_N\, dp_1 \cdots dp_N = \text{const}. \tag{3b}$$

In the above, $\Delta\Gamma[t]$ refers to any connected, moving collection of phase points. The $N - 2$ intermediate integrals—which we have not included—are written more naturally using differential forms, and we refer the reader to the text by Arnold [1] for a general discussion. These quantities are time (and canonical transformation) invariant.

However, if one wants to model the motion of particles which can be effectively created or destroyed, then the Liouville equation, Eq. (2), is not an appropriate description—even in the case where the particles themselves still follow Hamiltonian trajectories.

1.2. *The Generalized Liouville Equation*

As a simple example, consider the description of a one-dimensional plasma moving in an electrostatic potential field $\varphi(x, t)$. Further, assume that particles are injected into the system at a rate $S(v)$ and effectively removed by charge exchange with background neutrals at a rate $1/\tau_{cx}(v)$. Then, the relevant kinetic equation can be written

$$\frac{\partial f}{\partial t} + v\frac{\partial f}{\partial x} - \frac{\partial \varphi}{\partial x}\frac{\partial f}{\partial v} = S(v) - \frac{f}{\tau_{cx}(v)}. \tag{4}$$

Here, we emphasize that even though the trajectories (or characteristics) in the phase space $\Gamma = (x, v)$ are Hamiltonian, with

$$H(x, v, t) = \frac{v^2}{2} + \varphi(x, t), \tag{5}$$

the overall motion of the phase fluid is not incompressible. Thus, Eq. (2) is not sufficient to describe the dynamics in this case.

In the general case, one may allow for non-conservative effects—that is, nonconservation along the Hamiltonian

0021-9991/96 $18.00

flow $\dot{\Gamma}$—by considering f to satisfy a *generalized Liouville equation*,

$$\dot{f} = \frac{\partial f}{\partial t} + \dot{\Gamma}_i \frac{\partial f}{\partial \Gamma_i} = \Omega(f, \Gamma, t), \tag{6}$$

Here, the source function Ω denotes the rate of change of f along an orbit. Of course, it is evident that one must provide a further moment equation for the evolution of φ (i.e., a Poisson-type equation). We will discuss this point shortly. Nevertheless, the structure of Eq. (4) is indeed that of the generalized Liouville equation, Eq. (6).

In all but the simplest of systems, the specification of equations to supplement the set ($\dot{f}$, $\dot{\Gamma}$) will be required. Specifically, the evolution of the Hamiltonian system may depend on any number of "external" quantities, such as plasma waves, whose evolution is determined self-consistently by the form of the distribution function f (through moment equations, or otherwise). For example, we could close the one-dimensional system described above by specifying an independent differential equation for the evolution of $\varphi(x, t)$. Whatever the procedure, the motion in the (x, v)-plane remains that of an explicitly time *dependent* Hamiltonian system.

In Section 2, we describe a general method to solve Eq. (6) by following an ensemble of Hamiltonian trajectories numerically. This method decomposes the distribution f into continuous and discrete parts according to a low-noise δf scheme [2–6]. In Section 3, the method is applied to the classic bump-on-tail problem, and in Section 4, a simulation of the toroidicity-induced Alfvén eigenmode (TAE) is described. We include a brief discussion of considerations related to the time integration scheme in Section 5. A summary is given in Section 6.

2. THE HAMILTONIAN TRAJECTORY METHOD

The present algorithm was inspired by the work of Parker and Lee [2], who outlined a related scheme for the gyrokinetic simulation of drift-waves. This technique falls into the same general class as any of the so-called δf algorithms [3], which have found considerable success in the form of low-noise particle codes for the solution of the gyrokinetic equation and for the study of the linear and nonlinear evolution of TAE modes [4]. Indeed, it is now well-recognized that δf-methods offer a substantial improvement in accuracy over traditional simulations in cases where the particle distribution is only weakly modified from a "background" which is specified analytically. A systematic kinetic theory to quantify the noise intensity reduction in δf simulations has also been recently developed by Hu and Krommes [5].

The formulation presented in this paper arose through attempts to devise a particle simulation code to study the nonlinear dynamics of the TAE. The challenge presented a number a difficulties which were not properly resolved in the existing literature—such as the evaluation of moments of $f = f_0 + \delta f$, as well as a rigorous description of transformations between loaded, canonical, and noncanonical spaces. In what follows, a formulation is presented which is very flexible and can be applied directly to either the simple 1D bump-on-tail problem, or to the more complicated TAE problem.

2.1. *Derivation*

For systems of interest in plasma simulation, it is often the case that f will differ only slightly from some known analytic distribution f_0—the difference arising through localized wave-particle interaction. In cases where f is only weakly distorted, it can be shown [5] that the δf separation results in a reduction of order $|\delta f/f|^2$ in numerical "noise intensity." This factor was originally postulated by Kotschenreuther [6] some years ago.

We will begin by formulating the algorithm for systems where the position and velocity-space coordinates are exactly canonical—for example, the (x, v) space of Eq. (5). Systems for which the configuration/velocity space variables are *not* canonical do arise and require additional generalization. We will discuss this point with reference to the TAE problem in Section 4.

Begin by decomposing $f(\Gamma, t)$,

$$f(\Gamma, t) = \underbrace{f_0(\Gamma, t)}_{\text{analytic}} + \underbrace{\delta f(\Gamma, t)}_{\text{markers}}, \tag{7}$$

where f_0 is a chosen analytic function, and δf will be represented by a discrete lattice of markers. The evolution of δf, when viewed as a functional $\delta f[\Gamma(t), t]$ on the infinite-dimensional "fluid" phase-space Γ, can then be approximated by the evolution of a finite-dimensional (n_p) set of markers:

$$\delta \dot{f}_j(t) = \Omega_j - \frac{\partial f_{0j}}{\partial t} - \sum_{i=1}^{2N} \dot{\Gamma}^i_j(t) \left[\frac{\partial f_0}{\partial \Gamma^i}\right]_{\Gamma^i = \Gamma^i_j}, \quad j = 1, ..., n_p. \tag{8}$$

The separation into analytic (f_0) and numerical (δf) components in no way presumes that the latter must be much "smaller" than the former. In fact, the separation is formally valid in all cases. However, when the condition $\delta f \ll f_0$ is satisfied, the simulation noise is expected to be substantially less than if the entire distribution were represented numerically.

The n_p equations above are supplemented by $2N \times n_p$ Hamiltonian marker equations

$$\dot{\Gamma}^i_j = F^i_j(\Gamma, Z(t)), \tag{9}$$

where the vector $Z(t)$ is any time-dependent function which appears in the Hamiltonian, but whose evolution is not governed by canonical equations. Z may be a simple analytic function, or conversely, a complicated function of time which must be calculated by numerical means. Moreover, the dimension of Z is in no way connected with the number of markers, and in Section 3 we will show how this function may be used to represent a spectrum of wave amplitudes and phases $\{A, \alpha\}$ in both the bump-on-tail and TAE problems.

Now, consider an arbitrary space $\mathscr{U}$, with $\mathrm{Dim}(\mathscr{U}) = 2N$, which is filled with lattice points in an asymptotically *uniform* way. Such a uniform space is related to the original phase space through

$$d\Gamma = \mathscr{M}(\mathscr{U})\, d\mathscr{U}, \tag{10}$$

where $\mathscr{M}$ is the determinant of the Jacobian matrix. With these definitions, it follows that integral operators transform as

$$\int f(\Gamma, t) g(\Gamma, t)\, d\Gamma \sim \int f_0(\Gamma, t) g(\Gamma, t)\, d\Gamma + \sum_{j=1}^{n_p} \delta f_j(t) g(\Gamma_j(t), t)\, \Delta\Gamma_i, \tag{11}$$

where we have defined the equivalent (time-independent) phase space marker volume

$$\Delta\Gamma_j \equiv \frac{V(\mathscr{U})}{n_p} \mathscr{M}_j \quad \text{with } V(\mathscr{U}) = \int d\mathscr{U}. \tag{12}$$

Note that in a conventional particle simulation, one would represent the entire distribution f as a sum over either point, or shaped, particles. In the present notation, this would imply $f_0 = 0$, and consequently, that $\delta f = 0$. Each δf_j would then be constant along the phase flow, with moments of f determined through the more familiar association

$$\int f(\Gamma, t) g(\Gamma, t)\, d\Gamma \sim \sum_{j=1}^{n_p} \delta f_j(0) g(\Gamma_j(t), t)\, \Delta\Gamma_j, \tag{13}$$

which is just a sum over weighted particles.

3. THE BUMP-ON-TAIL INSTABILITY

As a simple example, we apply the Hamiltonian trajectory algorithm to the bump-on-tail problem, using the Lagrangian formulation developed by Berk, Breizman, and Pekker [7]. This model describes the nonlinear interaction of energetic electrons with a spectrum of plasma modes. Since the nonlinearity of the bulk plasma is largely irrelevant for the growth and saturation of the unstable part of the spectrum, it is sufficient to consider the interaction of particles with "fixed" electrostatic modes. In doing so, the need to solve the Poisson equation is eliminated and replaced by evolution equations for only the amplitude and phase of each discrete mode. Analytic features of this model have also been calculated [8]. In the study of wave–particle interaction, the bump-on-tail problem emerges as an important paradigm, with many features in common with more complicated stability problems, such as that posed by fast-particle-driven modes in tokamaks (i.e. fishbones or TAE modes).

3.1. *Formulation in Terms of the Characteristic Method*

Throughout this example, we will restrict our discussion to the case of one wave. We will use the wave variables (P, Q) (which correspond formally to Z of Eq. (9)) such that the amplitude A and phase α are given by $P = A \cos \alpha$ and $Q = A \sin \alpha$. The wave–particle interaction equations (not yet in δf form), including a background wave damping rate, γ_d, are [7]

$$\dot{x}_j = v_j, \tag{14a}$$

$$\dot{v}_j = Q \cos(x_j - t) - P \sin(x_j - t), \tag{14b}$$

$$\dot{Q} = -\gamma_d Q - \frac{1}{n_i} \sum_{j=1}^{n_p} q_j \cos(x_j - t), \tag{15a}$$

$$\dot{P} = -\gamma_d P + \frac{1}{n_i} \sum_{j=1}^{n_p} q_j \sin(x_j - t), \tag{15b}$$

where n_i is the number of plasma ions and $\sum_j q_j = n_b$ is the number of beam ions, with each q_j the "macroparticle weight." Clearly, the space $\Gamma = (x, v)$ is canonical. We can now construct the δf system, with a source and sink: given an initial distribution $f_0(v)$ annihilation rate ν and source $S(v) = \nu f_0(v)$, we replace Eqs. (15a), (15b) by

$$\dot{Q} = -\gamma_d Q - \frac{1}{n_i} \sum_{j=1}^{n_p} \delta n_j \cos(x_j - t), \tag{16a}$$

$$\dot{P} = -\gamma_d P + \frac{1}{n_i} \sum_{j=1}^{n_p} \delta n_j \sin(x_j - t), \tag{16b}$$

$$\delta\dot{n}_j = -\dot{v}_j f_0'(v_j)\, \Delta\Gamma_j - \nu\, \delta n_j, \tag{17}$$

The δf-system is represented collectively by Eqs. (14) (marker equations of motion), Eqs. (16) (wave evolution equations), and Eq. (17). In the above, we have introduced the functions $\delta n_j \equiv \delta f_j \Delta\Gamma_j$, with $\Delta\Gamma_j = \mathscr{M}_j / n_p$ (below, $V(\mathscr{U})$ is taken to be unity). Each δn_j is analogous to an effective

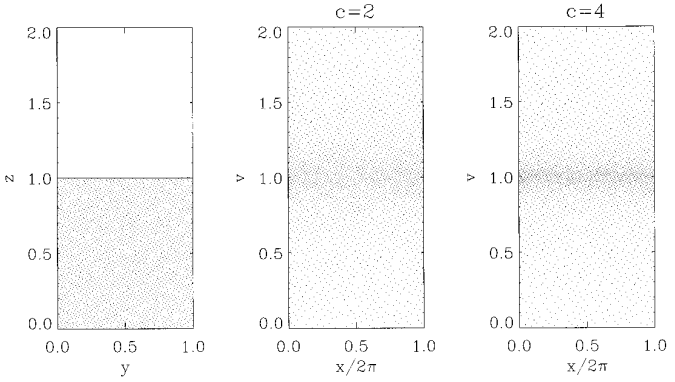

FIG. 1. Marker distributions generated using the sequence defined by Eq. (A1): (a) Uniform distribution on the unit square; (b) resonance-loaded distribution, Eqs. (23) and (24), for $c = 2$; and (c) for $c = 4$.

"particle fluctuation," with the total number of beam particles $n_b = \int f_0\, d\Gamma \sim \sum_j f_{0j}\, \Delta\Gamma_j$. Frequency and wavelength have been normalized so that the resonant velocity is $v = 1$.

For the simulation, we will use a smooth initial distribution defined over the interval $0 \le v \le 2$. This avoids any difficulty with reactive contributions coming from a distribution which goes discontinuously to zero at the endpoints. Choosing

$$f_0(v) = Cv^4(2 - v)^2, \tag{18}$$

with C a normalization constant, yields an unstable mode with linear growth rate

$$\gamma_L = \pi^2 \frac{f_0'(1)}{n_i} \equiv \pi^2 \beta. \tag{19}$$

It is easy to verify that $\beta = (105/128\pi)(n_b/n_i)$. Equation (19) is valid for γ_L much smaller than the characteristic width of $f'(v)$ (that is, $\gamma_L \ll |f'/f''|$). Otherwise, resonant particles away from $v = 1$ contribute to the growth rate, and a more complicated integral over f' is required.

Now, fill the unit square (y, z) with points using the method of Appendix A, as illustrated in Fig. 1a; then map these points to the (x, v) space ($0 \le x \le 2\pi$ and $0 \le v \le 2$) according to

$$x = 2\pi y, \tag{20a}$$

$$v = \frac{2z(1 + c(3 - 6z + 4z^2))}{1 + c}. \tag{20b}$$

This gives a loading preferentially weighted along $v = 1$, in proportion to the value of c (with $c = 0$ uniform, and increasing values more concentrated along $v = 1$). Examples for $c = 2, 4$ are shown in Figs. 1b and 1c. The Jacobian in this case is simply

$$\mathcal{M} = 4\pi \frac{1 + 3c(1 - 2z)^2}{1 + c}. \tag{21}$$

3.2. *Linear Growth Rate and Saturation*

For the time integration of Eqs. (14), (16), and (17), we use a fourth-order Adams predictor [9]. Since the δf form of the equations is *not* Hamiltonian, special symplectic integration methods [10–11] are not applicable, although it is conceivable that hybrid or other specialized methods may, in the future, be developed. We will discuss this point further in Section 5.

The first test for the efficiency and accuracy of the algorithm is to reproduce known values for the linear growth rate γ_L and the mode saturation ratio $c_L = \omega_t/\gamma_L$ (with $\omega_t = \sqrt{A}$, and $c_L \sim 3.3$). Figure 2 shows the results of a 5000-particle simulation, where the numerical growth rate and saturation amplitude agree precisely with theory. The number of particles used is very small by comparison with non-δf methods. The latter, it should be emphasized, require an increasing number of particles to overcome noise from the numerical representation of f_0 as γ_L is decreased (compare with the 512,000-particle simulation of Cary and Doxas [10]). Due to the intrinsic scaling of the RHS of Eq. (14b) and thus Eq. (17) with the wave amplitude, we can choose β as small as we like (obvious numerical requirements, such as $|\dot{A}/A| > 10^{-15}$, notwithstanding) and the model equations will capture precisely the linear dynamics. For example, it is possible to accurately track the linear evolution of a mode which carries less energy than a single resonant particle.

Once the wave has saturated, many more markers are

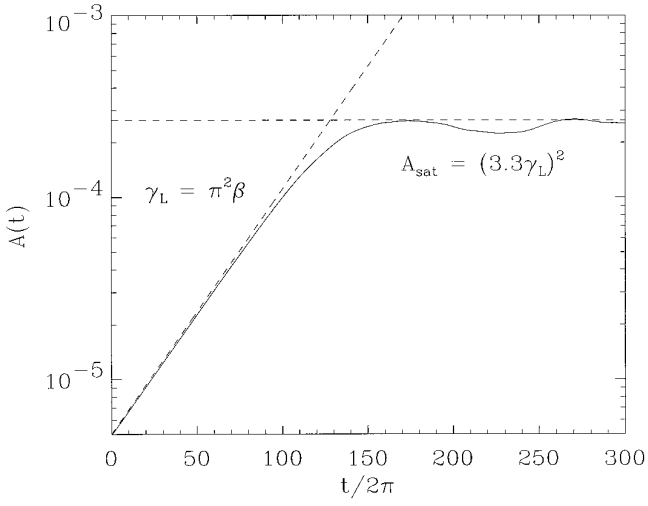

FIG. 2. Linear evolution and subsequent nonlinear saturation of a single mode, determined by solving Eqs. (20) for $\beta = 5 \times 10^{-4}$ and $\gamma_d = \nu = 0$ with $n_p = 5000$ markers. Dashed curves show analytic predictions for linear evolution and saturated amplitude.

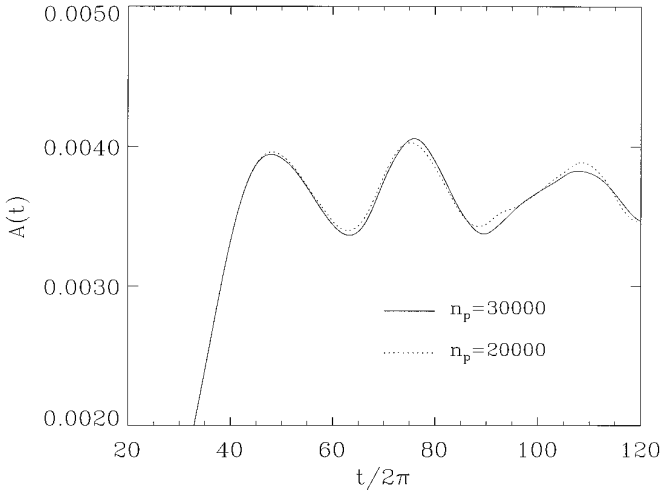

FIG. 3. Comparison of nonlinear oscillations of the saturated wave for $n_p = 20000$ and 30000 and $\beta = 2 \times 10^{-3}$. A small phase shift occurs due to finite marker number.

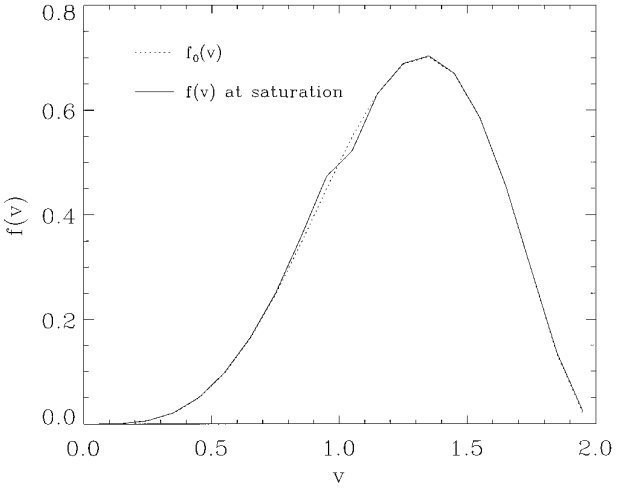

FIG. 4. Comparison of equilibrium and saturated distributions for the simulation of Fig. 3 ($n_p = 30000$). Flattening at the resonant velocity $v = 1$ is clearly evident.

required, in general, to resolve the small-amplitude nonlinear oscillations. We have observed that after the wave saturates and begins executing quasi-periodic nonlinear oscillations, a slow phase decorrelation becomes evident in simulations with differing marker numbers. Because the simulations are converged with respect to integrator time step, the difference is due solely to the nondense marker covering of phase space. Consequently, as the number of markers is further increased, convergence can be expected for a finite time only, as infinitesimally nearby markers in the vicinity of a separatrix will diverge exponentially due to turbulent mixing of phase volume. This phenomenon is illustrated in Fig. 3, for $\beta = 2 \times 10^{-3}$, where simulations with 20000 and 30000 markers are compared. Visual differences, as we have indicated, are not affected by a decrease in time step. As the wave saturates, the particle distribution is flattened in the vicinity of the resonant velocity $v = 1$, as illustrated in Fig. 4.

3.3. *Particle and Energy Conservation*

Consider first the special case $\gamma_d = \nu = 0$. Here, we expect the total particle number in the corresponding physical system to be time invariant (since $\nu = 0$). However, this invariance is not exactly realized in the numerical method for a finite number, n_p, of markers due to discretization error. If we begin with $\delta f = 0$ (i.e., all $\delta n_j(0) = 0$), then

$$n_b = \int f_0(v)\, dx\, dv \quad \text{(initial number)}, \tag{22a}$$

$$\delta n(t) = \sum_{j=1}^{n_p} \delta n_j(t) \quad \text{(fluctuation)}, \tag{22b}$$

with the total number $n(t) = n_b + \delta n(t)$. In the limit $n_p \to \infty$, we expect $\delta n = 0$ to obtain, thus satisfying the requirement of particle conservation. In general, these conclusions indicate that one should consider the size of the relative fluctuation $\delta n/n_b$ as a simple and useful measure of code accuracy and convergence—as well as a means of detection of coding error. Indeed, Parker and Lee [2] encountered poor convergence of the RMS fluctuation of δn with increasing particle number. This was the result of a very subtle error in the formulation of their nonlinear weighting scheme, as pointed out by Krommes and Hu [5]. Figure 5 shows a plot which illustrates the convergence of

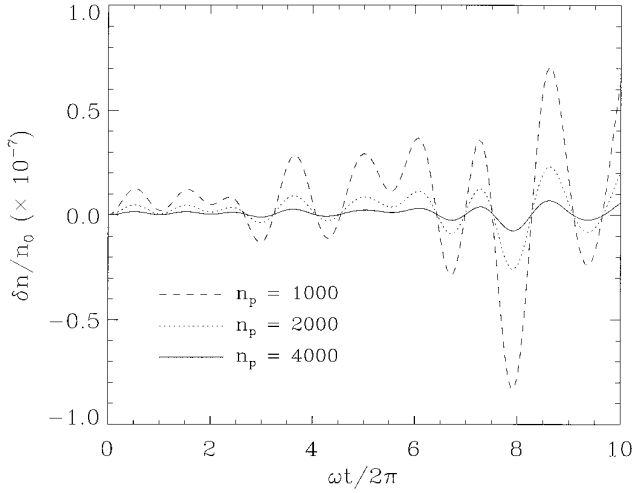

FIG. 5. Relative fluctuation in particle number for a series of runs with $n_p = 1000$, 2000, and 4000 for $\beta = 5 \times 10^{-4}$. In this case, we expect $\delta n \to 0$ as $n_p \to \infty$ to reflect particle conservation in the continuous Liouville system.

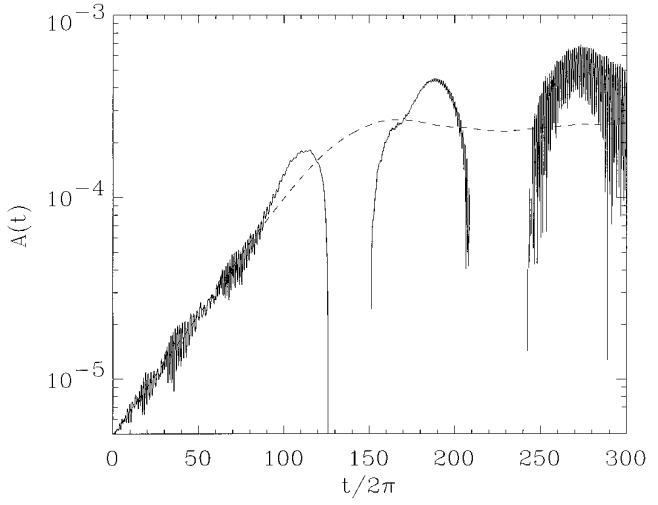

FIG. 6. Evaluation of $A(t)$ using the energy integral, Eq. (24) (solid curve) compared with differential update, Eqs. (16a), (16b) (dotted curve). Parameters are the same as in Fig. 1.

$\delta n/n_b$ as n_p is increased. Generally, the amplitude of the fluctuation increases in rough proportion to the wave amplitude.

A relatively important feature of the algorithm is the differential form of the amplitude update given by Eqs. (16a), (16b). To see this, consider the case of a single mode in the non-δf formalism. One can form the following identity directly from Eqs. (15) (with $\gamma_d = 0$):

$$\left(\frac{P^2}{2} + \frac{Q^2}{2}\right) + \beta \sum_{j=1}^{n_p} q_j v_j = \text{const.} \tag{23}$$

This quantity represents the exact conservation of momentum. In fact, this equation also reflects conservation of system energy, to the extent that $d(v^2/2)/dt = v\dot{v} \sim \dot{v}$ for resonant particles. The identity, Eq. (23), evidently represents an algebraic method for the update of the wave amplitude according to

$$A(t)^2 \sim A(0)^2 - 2\beta \sum_{j=1}^{n_p} \delta n_j v_j. \tag{24}$$

However, plotting the right-hand side of Eq. (24) in Fig. 6, we obtain a very surprising result. For a moderate number of markers, the above-weighted sum over marker momenta is a *rapidly* oscillating function of time—much noisier than the amplitude as determined from the differential equations, Eqs. (16a), (16b). The oscillations present in the solid curve of Fig. 6 indicate a high level of statistical noise. Although the agreement improves as required when n_p increases (or, notably, as γ_L increases), one must conclude that an extra degree of "smoothing" is obtained from a differential update.

3.4. *Source, Sink, and Wave Damping*

The addition of a particle source, S, relaxation rate, ν, and background damping rate γ_d to the model represents a nonconservative generalization to the overall dynamics. When these parameters are finite, two possible wave evolution scenarios are possible. The first is steady-state saturation and occurs roughly when the relaxation rate exceeds the background damping rate. However, in the opposite limit of strong background damping, "bursting" of the wave amplitude may result. Both these phenomena occur on time scales much longer than the linear growth phase and are relatively difficult to resolve numerically. We concentrate on the steady-state regime, for which Berk and Breizman [8] have calculated the following estimate of the ratio of trapping frequency to linear growth rate:

$$\frac{\omega_t}{\gamma_L} = 1.9 \frac{\nu}{\gamma_d}. \tag{25}$$

Comparison of the numerical model with this estimate is illustrated in Fig. 7, where a slow approach to the steady-state value is in fact observed.

4. THE TAE

The toroidicity-induced Alfvén eigenmode (TAE) is a global, weakly damped magnetohydrodynamic mode which exists only in toroidal plasmas. Experimental observations have shown that MeV-fast ions—produced by ion-

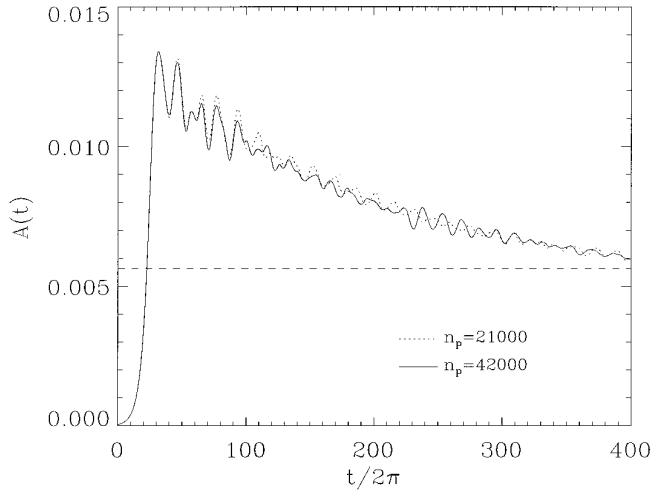

FIG. 7. Slow relaxation to steady-state wave amplitude in the presence of finite dissipation ($\gamma_d = \nu = 0.001$) for $\beta = 0.004$. Dashed horizontal line shows the analytic estimate, Eq. (25), for the steady-state value.

cyclotron resonance heating and neutral beam heating [12]—can destabilize the TAE. As a result, there is concern that it will be similarly unstable to the alpha particle populations present in a burning plasma [12]. Possible consequences are prompt alpha loss from the plasma into the first wall (with consequent wall damage), as well as collective instabilities causing alpha profile redistribution and poorer-than-expected alpha heating. Resolution of these transport and confinement issues hinges upon fast, accurate calculation of the both the growth rate and saturated amplitude of these modes.

For simplicity, we consider only the gyro-averaged motion of fast particles. There are four non-trivial dynamical variables in this motion: the velocity component along the magnetic field, $v_\parallel$, as well as three spatial coordinates, (φ, θ, ψ)—the toroidal angle, poloidal angle, and poloidal flux—which are determined by the equilibrium magnetic field structure. While tokamak equilibria must in general be calculated numerically, we will adopt an analytic equilibrium which is appropriate for circular cross section and large-aspect-ratio [13]:

$$\mathbf{B} = \nabla\varphi + I\nabla\theta \quad \text{with } B = \frac{(1 + (r/q)^2)^{1/2}}{1 + r\cos\theta}. \tag{26}$$

Here, $I \equiv r^2/q$ and $d\psi_t = r\,dr = q\,d\psi$, with ψ the poloidal flux, ψ_t the toroidal flux, and $q(\psi)$ the safety factor. The last quantity is arbitrary within the context of the present discussion. Also, here and in subsequent formulae, B is normalized to its value at $\psi = 0$.

4.1. *Guiding Centre Hamiltonian*

We choose dimensions such that the fast particle mass, m, the major radius, R_0, and the cyclotron frequency, ω_c, are unity. Then, the guiding center Hamiltonian takes the form [13]

$$H_{\rm gc}(P_\varphi, P_\theta, \varphi, \theta, \mu, t) = \frac{v_\parallel^2}{2} + \mu B + \Phi, \tag{27}$$

with the magnetic moment, $\mu = v_\perp^2/2B$, an exact invariant for a given particle. Considering only a single (m, n)-helical component of a TAE perturbation, we can write

$$\Phi = [\,\mathscr{X}(t)\cos(\Theta) + \mathscr{Y}(t)\sin(\Theta)]\phi(\psi), \tag{28}$$

where $\Theta \equiv n\varphi - m\theta - \omega t$ is the phase angle of the wave, $\phi(\psi)$ is the radial mode envelope, and the pair ($\mathscr{X}$, $\mathscr{Y}$) are slowly varying amplitudes. In the limit of zero plasma pressure, the canonical toroidal and poloidal angular momenta become

$$\left.\begin{aligned} P_\varphi &= \rho - \psi \\ P_\theta &= I\rho + \psi_{\rm t} \end{aligned}\right\} \quad \text{with } \rho B = v_\parallel + \frac{k_{\parallel m}}{\omega}\Phi, \tag{29}$$

such that $k_{\parallel m} = n - m/q$ is the parallel wavenumber. The guiding center equations are obtained from the Hamiltonian, Eq. (27), in the usual way. In particular, it is important to note that $\rho = \rho(P_\varphi, P_\theta)$ and $\psi = \psi(P_\varphi, P_\theta)$. The invariant volume element connected with this flow is

$$d\Gamma = (2\pi\mu)\,dP_\varphi\,d\varphi\,dP_\theta\,d\theta. \tag{30}$$

4.2. *Algorithm for Numerical Simulation*

In toroidal geometry, the element of volume is usually obtained by forming a simple product of velocity and real-space elements,

$$d\Gamma^{(p)} \equiv d^3r\,d^3v = 2\pi v^2\,dv\,d\lambda\,\mathscr{J}\,d\psi\,d\varphi\,d\theta, \tag{31}$$

where $\mathscr{J}$ is the Jacobian connecting real-space coordinates to the straight-line (generally nonorthogonal) coordinates (φ, θ, ψ):

$$\mathscr{J} = \frac{1}{|\nabla\psi\cdot(\nabla\theta\times\nabla\varphi)|} = \frac{I + q}{B^2}, \tag{32}$$

and $\lambda \equiv v_\parallel/v$ is the cosine of the pitch angle. A factor of 2π arises in $d\Gamma^{(p)}$ from an integration over gyrophase. The volume element $d\Gamma^{(p)}$ is *not* canonical and as a consequence, the distribution $f^{(p)}$ of phase points on this element does *not* satisfy the Liouville equation. However, it can be seen that

$$f^{(p)}\,d\Gamma^{(p)} = \underbrace{f^{(p)}\,\mathscr{N}}_{f}\,d\Gamma, \tag{33}$$

such that f *does* satisfy the Liouville equation. Here, $\mathscr{N}(t)$ is the determinant of the Jacobian matrix

$$\mathscr{N}(t) \equiv \left|\frac{\partial\Gamma^{(p)}}{\partial\Gamma}\right| = \frac{\mathscr{J}B^2}{D}, \tag{34}$$

with $D \equiv \rho\,dI/d\psi + I + q$. Thus, in general, the kinetic equation for $f^{(p)}$ will contain an additional term due to $\mathscr{N}$. For fast ions in a tokamak, however, the Jacobian $\mathscr{N}$ is very close to unity. In this case, we can sidestep the present difficulty by simply specifying f, rather than $f^{(p)}$. In doing so, the evolution of $\mathscr{N}$ remains implicit. Normalization constants (such as the total number and pressure of fast-particles, $n_{\rm f}$ and $\beta_{\rm f}$) can still be computed using $f^{(p)}$ in the usual way with negligible error.

In the absence of a plasma wave ($\Phi = 0$), the fast particle motion will conserve both energy, $H_{\rm gc}$, and toroidal mo-

mentum, P_φ. The unperturbed distribution of fast particles is accordingly restricted to be a function of these motion invariants. To calculate the evolution of the fast particle distribution in the presence of a perturbation, we decompose the exact distribution f as

$$f = \underbrace{f_0(\mathscr{E}, P_\varphi; \mu)}_{\text{analytic}} + \underbrace{\delta f(\Gamma, t)}_{\text{markers}}, \tag{35}$$

where $\mathscr{E} = \mathscr{E}(P_\varphi, P_\theta, \theta)$ is defined as $\mathscr{E} \equiv \rho^2 B^2/2 + \mu B$. This definition ensures that the initial number of particles, n_0, is time-invariant:

$$n_0 \equiv \int f_0(\mathscr{E}, P_\varphi; \mu)\, d\Gamma = \text{const}, \tag{36}$$

with the deviation evolving according to

$$\dot{\delta f} = -\dot{P}_\varphi \frac{\partial f_0}{\partial P_\varphi} - \dot{\mathscr{E}} \frac{\partial f_0}{\partial \mathscr{E}}. \tag{37}$$

This equation has the desired property that the evolution of δf is driven only by the wave perturbation, such that the average of the RHS is nearly zero for all but a small fraction of resonant particles. Note that if one were to specify $f^{(p)}$, rather than f, as we have indicated, the presence of an $\mathscr{N}\dot{}$ term would spoil this desireable property.

In order to represent δf numerically, we begin by filling an arbitrary space $\mathscr{U}$ with a four-dimensional point set and then relating this set to the corresponding element in Γ as per Eq. (10). It should be clear that the choice of $\mathscr{U}$ is *not* unique and may be altered to suit a particular simulation. A simple choice is

$$d\mathscr{U} = d\psi\, dv\, d\lambda\, d\varphi\, d\theta \quad \text{so that } \mathscr{M} = \frac{2\pi v^2 D}{B^2}. \tag{38}$$

Equation (12) can once again be used with

$$V(\mathscr{U}) = (2\pi)^2(\lambda_{\max} - \lambda_{\min})(\psi_{\max} - \psi_{\min})(v_{\max} - v_{\min}). \tag{39}$$

Defining δn_j as in Eq. (17), the wave equations are

$$\dot{\mathscr{X}} = -\frac{1}{2\mathrm{E}} \sum_{j=1}^{n_p} \delta n_j(\omega - k_{\|m}\rho_j B_j) \sin(\Theta)\phi(\psi), \tag{40a}$$

$$\dot{\mathscr{Y}} = \frac{1}{2\mathrm{E}} \sum_{j=1}^{n_p} \delta n_j(\omega - k_{\|m}\rho_j B_j) \cos(\Theta)\phi(\psi). \tag{40b}$$

The non-δf forms, from which these were obtained, can be derived by following the presentation in [14]. Above, E is a normalization constant related to the inertial energy of the mode. Another subtle but important point is the absence of f_0 in the wave equations, Eqs. (40). Because f_0 is axisymmetric (no φ-dependence), the first integral on the RHS of Eq. (11) vanishes. In other words, for any $g(P_\varphi, P_\theta, \theta, \mu, t)$, we have

$$\int_0^{2\pi} g(P_\varphi, P_\theta, \theta, \mu, t) \sin(n\varphi - m\theta - \omega t)\, d\varphi = 0. \tag{41}$$

This completes the description of the TAE model. The result is a $(5\ n_p + 2)$D system of ordinary differential equations: $\{\dot{P}_{\varphi j}, \dot{\psi}_j, \dot{\varphi}_j, \dot{\theta}_j, \dot{\delta f}_j\}$, for $j = 1, ..., n_p$, along with $\{\dot{\mathscr{X}}\ \dot{\mathscr{Y}}\}$. Note that we have chosen to integrate ψ forward in time instead of P_θ. This is the preferred coordinate for guiding center simulations since $P_\theta = P_\theta(\psi)$. Otherwise, an implicit equation must be inverted to determine ψ.

4.2. *Simulation Results*

We first consider the linear growth phase of a wave using the beam distribution

$$f_0 = C \exp\left(-\alpha \frac{\langle\psi\rangle}{\psi(a)}\right) \exp\left(-\frac{\mathscr{E}}{T}\right) \delta\left(\frac{\mu}{\mathscr{E}}\right), \tag{42}$$

with $\langle\psi\rangle \equiv \mathscr{E}^{1/2} - \mathscr{P}$ an "orbit-averaged" measure of the poloidal flux valid for passing particles, and $\psi(a)$ the flux at the plasma edge, $r = a$. A single $(n, m) = (5, 7)$ helical perturbation in a high-field, large-aspect-ratio ($a = 80$ cm, $R_0 = 800$ cm) equilibrium was considered. The extreme parameter values were chosen so that results would lie well within the small-orbit-width, large-aspect-ratio regime, and thus be amenable to comparison with analytic formulae. The time integration was performed using a fourth-order Adams predictor method, although the more general version of the nonlinear code—which must cope with trapped particles and marker losses—uses a fourth-order Runge–Kutta (RK) method.

We set $\alpha = 2.5$ and $T = 1.76$ MeV and made a scan of growth rate versus magnetic field strength. Figure 8 shows the results, for both "unlocked" and "locked" wave frequency. The frequency-locked evolution is obtained operationally by fixing $\mathscr{Y} \equiv 0$—a standard approximation of linear theory. In reality, as the drive increases, a frequency shift is induced which (in the unlocked-frequency case) modifies the resonance condition and consequently the growth rate. Figure 8 shows that the frequency shift in this case leads to a decrease in the growth rate. We emphasize that these results were computed with the wave amplitude many orders of magnitude smaller than the saturated state—so that wave-particle nonlinearity is negligible.

In Fig. 8 the δf results, each computed using 60000 markers, are compared with both an analytic approximation (which treats finite-orbit-width effects perturbatively), as

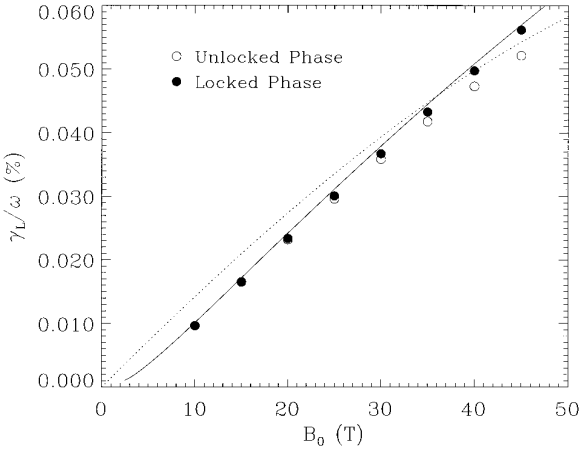

FIG. 8. Comparison of linear growth rates for a beam-driven TAE. The dots are δf simulation results (with solid dots for locked phase and open circles for unlocked phase). The solid curve is the numerical result from an independent δW code, and the dashed line was calculated using a zero-orbit-width analytic formula.

well as with the growth rate calculated by an independent numerical linear δW code. Such cross-code comparisons are of inestimable value for error-detection. The agreement between codes indicated in Fig. 8 is exceptional. Moreover, in terms of execution time, the fully nonlinear initial-value δf code is suprisingly competitive with the linear δW code for calculation of γ_L/ω.

As a final illustration of the application of the δf method, Fig. 9 shows a 60000 marker simulation of the growth and saturation of an $m = (8, 9)$, $n = 10$ TAE mode driven by an isotropic distribution of alpha particles in a realistic, ITER-like plasma. This should be compared with Fig. 9 of [4], which shows a 100000 marker δf simulation of the same system for a simpler $n = 3$ perturbation.

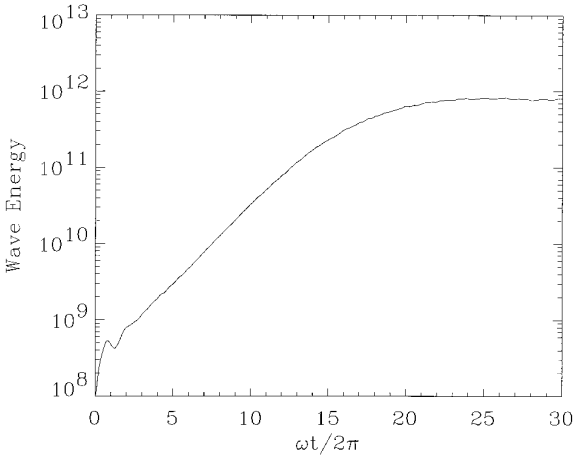

FIG. 9. Growth and saturation of an $n = 10$, $m = (8, 9)$ TAE mode in an ITER-like plasma, calculated using $n_p = 60000$. The fast particle distribution is isotropic and slowing-down in velocity, with a realistic spread around the alpha birth energy. The alpha pressure gradient is peaked around $r/a \sim 0.5$.

5. CHOICE OF INTEGRATION METHOD

The choice of time integration method is clearly an important concern for the development of a fast simulation code. Substantial improvements in performance and accuracy over typical adaptive Runge–Kutta (RK) or predictor–corrector (PC) methods are achievable in traditional (non-δf) particle codes [10] through the use of symplectic integration algorithms (SIA) [11]. Unfortunately, these algorithms are not applicable to the δf systems of this paper, since the system of ordinary differential equations is not Hamiltonian.

With regard to the simulation of toroidal plasmas, there is no known factorization of the guiding center Hamiltonian into a product of integrable Lie maps, so that an explicit SIA of second or higher order does not exist. Furthermore, restrictions on the integrator are imposed by particle losses and origin crossings (the latter situation requiring a change of coordinate system). These considerations led to the choice of an RK method for the general TAE integrator, although integration of simple passing orbits indicated that the more cumbersome Adams predictor step was slightly faster for a given accuracy.

6. SUMMARY AND CONCLUSIONS

In this paper we have developed a systematic numerical approach to solve the generalized Liouville equation, which makes use of a numerical grid defined by the Hamiltonian trajectories of the associated conservative system, along with a δf decomposition of the distribution function. The applicability of the method to systems which may have nonconservative degrees of freedom (i.e., waves subject to background dissipation), as well as to systems whose position and velocity coordinates are not exactly canonical, has also been demonstrated. Various numerical tests have been performed using discrete particle models of the bump-on-tail and TAE instabilities. These show excellent agreement with independent calculations of the growth rate and (for the bump-on-tail problem) saturation amplitude.

APPENDIX A: NONRANDOM MARKER LOADING

A simple procedure exists for filling the space $\mathscr{W}$ with low-noise point sets. This method and the associated problem of particle loading are described in detail by Denavit and Walsh [15]. The utility of this method stems from the avoidance of "beaming"-type instabilities which occur when loading on a regular lattice, while still maintaining

a higher degree of uniformity than a random population. Such a distribution enables a ''quiet-start'' to the simulation—something which is particularly useful for the calculation of linear growth rates and other early-time phenomena.

Let $\mathscr{U}$ be the M-cube, and define

$$\mathscr{U}_i \equiv \left\{ \frac{i}{n_p}, \phi_{P(1)}(i), ..., \phi_{P(M-1)}(i) \right\}, \quad i = 0, ..., n_p - 1, \tag{A1}$$

as a sequence of n_p points in this cube, where $P(j)$ is the jth prime ($P(1) = 2$, $P(2) = 3$, etc.). The function $\phi_b(i)$ is calculated by inverting the base b representation of i in the following manner:

$$\text{if } i = a_0 + a_1 b + a_2 b^2 + \cdots \quad \text{then } \phi_b(i) \equiv \frac{a_0}{b} + \frac{a_1}{b^2} + \cdots. \tag{A2}$$

Since the sequence defined by Eq. (A1) is in general quasi-periodic with period

$$n_0 = P(1) \cdots P(M-1), \tag{A3}$$

we should choose n_p to be an integer multiple of n_0. An example for $M = 2$ and $n_p = 3000$ is shown in Fig. 1a.

ACKNOWLEDGMENTS

The author is indebted to D. N. Borba for the δW calculation of Fig. 8, as well as for a substantial number of interesting and helpful discussions. Thanks also to H. L. Berk and B. N. Breizman for providing the both the motivation and the actual formalism to study the nonlinear problems discussed in this paper and to S. E. Sharapov and R. A. M. Van der Linden for reading an early version of the manuscript. Financial assistance from the Natural Sciences and Engineering Research Council of Canada is gratefully acknowledged.

REFERENCES

1. V. I. Arnold, *Mathematical Methods of Classical Mechanics*, 2nd ed. (Springer-Verlag, New York, 1989), p. 201.
2. S. E. Parker and W. W. Lee, *Phys. Fluids B* **5,** 77 (1993).
3. R. E. Denton and M. Kotschenreuther, *J. Comput. Phys.* **119,** 283 (1995).
4. Y. Wu, R. B. White, Y. Chen, and M. N. Rosenbluth, *Phys. Plasmas* **2,** 4555 (1995).
5. G. Hu and J. A. Krommes, *Phys. Plasmas* **1,** 863 (1994).
6. M. Kotschenreuther, *Bull. Am. Phys. Soc.* **34,** 2107 (1988).
7. H. L. Berk, B. N. Breizman, and M. Pekker, *Phys. Plasmas* **2,** 3007 (1995).
8. H. L. Berk and B. N. Breizman, *Phys. Fluids B* **2,** 2246 (1990).
9. P. Henrici, *Discrete Variable Methods in Ordinary Differential Equations* (Wiley, New York, 1962), p. 187.
10. J. R. Cary and I. Doxas, *J. Comput. Phys.* **107,** 98 (1993).
11. E. Forest and R. Ruth, *Physica D* **43,** 105 (1990); J. Candy and W. Rozmus, *J. Comput. Phys.* **92,** 230 (1991).
12. W. W. Heidbrink *et al.*, *Phys. Rev. Lett.* **71,** 855 (1993); H. Kimura *et al.*, *Japan J. Plasma Fusion Res.* **71,** 1147 (1995); J. Candy and M. N. Rosenbluth, *Nucl. Fusion* **35,** 1069 (1995).
13. R. B. White and M. S. Chance, *Phys. Fluids* **27,** 2455 (1984).
14. H. L. Berk, B. N. Breizman, and M. Pekker, *Nucl. Fusion* **35,** 1713 (1995).
15. J. Denavit and J. M. Walsh, *Comments Plasma Phys. Controlled Fusion* **6,** 209 (1981).